Int. J. Heat Mass Transfer. Vol. 36, No. 15, pp. 3765–3771, 1993
Printed in Great Britain

0017–9310/93 $6.00 + 0.00

Experimental investigation of leakage in shell-and-tube heat exchangers with segmental baffles

W. ROETZEL and D. LEE

Institute of Thermodynamics, University of the Federal Armed Forces Hamburg, D-22039 Hamburg, Germany

(*Received* 5 *October* 1992 *and in final form* 1 *March* 1993)

Abstract—Thermal performance in shell-and-tube heat exchangers with segmental baffles has been experimentally investigated concerning five variables: stream flow direction, shell-side flow rate, tube-side flow rate, clearance between baffles and shell, and distance between baffles. The axial dispersion model has been applied to predict properly the actual thermal performance in the shell-and-tube heat exchanger. The shell-side dispersive Péclet number *Pe* depends only on the clearance between baffles and shell and on the distance between baffles, while the same heat transfer correlations can be used in all cases.

INTRODUCTION

THE CONVENTIONAL calculation of thermal performance in shell-and-tube heat exchangers with segmental baffles is usually based on the ideal simplifying assumptions that the shell-side flow in any cross-section of its flow path is completely transversely mixed (plug flow) and the temperature depends only on the axial coordinate. The real flow pattern on the shell side is very complex. There exist different flow paths and regions of stagnation. The velocity of the main stream across the tube banks is nonuniform and deviates from the ideal model [1].

Tinker analyzed the different flow paths, which consist of one main cross-flow stream and several bypass streams with different thermal performances on the shell-side of baffled heat exchangers, and he developed a complicated model with a simplified rating system to predict the shell-side performance in the heat exchanger [2, 3]. This model was later improved by Palen and Taborek [4] who introduced a correction factor for the effective mean temperature difference, and concluded that the shell–baffle leakage flow stream (Tinker's stream *E* [2]) has the most important effect on this correction factor. For a single-pass exchanger, Mueller [5] proposed the bypass model, which considers the influence of bypassing or leakage on the average effective mean temperature difference. The cell method developed by Gaddis and Schlünder [6] divides the shell-side flow into main stream and leakage stream, which affect the heat transfer coefficient through their portion. Diaz and Aguayo [7] were the first who introduced axial dispersion effects and suggested a dispersion model between perfect mixing and plug flow. However, no information is available on how the dispersion coefficient depends on the flow distribution.

The analytical thermal rating method for shell-and-tube heat exchangers with one shell-side pass and arbitrary number and size of tube passes was developed by Roetzel and Spang for the plug flow model [8]. With the concept of axial dispersion, they have investigated the thermal performance of segmentally baffled shell-and-tube heat exchangers (TEMA E-type) under different boundary conditions [9]. Later, the dispersion model was further developed and applied to split-flow (G-type) [10, 11] and divided-flow (J-type) [10, 12] as well as to transient processes in E-type shell-and-tube heat exchangers [13].

The purpose of this work is to investigate experimentally the influence of leakage flow between baffles and shell, the effect of the actual flow pattern and of different distances between baffles on the thermal performance in shell-and-tube heat exchangers with segmental baffles. Furthermore, the empirical heat transfer correlations are developed which can be used together with the dispersion model to predict thermal performance of shell-and-tube heat exchangers.

EXPERIMENTS

Apparatus and instrumentation

The overall experimental assembly, which consists of two closed operation cycles with distilled water, is shown in Fig. 1. The two operation cycles, the cold medium cycle with dashed lines and the hot medium cycle with solid lines, will transfer heat in the test heat exchanger denoted as W1 in Fig. 1. The hot medium flows through the tubes of the test heat exchanger and is transported by centrifugal pump (P2) with digital speed controlling regulator. The distilled water is first heated by four 22.5 kW electrical heaters with adjustable heating power in stages. The last heater is connected to a temperature controller, with which the inlet temperature of tube-side water is regulated

NOMENCLATURE

A	heat transfer surface area [m^2]
A^*	flow cross-sectional area [m^2]
C_1, C_2	constants
D_i	inside shell diameter [m]
d_a	outside tube diameter [m]
d_i	inside tube diameter [m]
E	dispersive thermal conductivity [$W m^{-1} K^{-1}$]
h	heat transfer coefficient [$W m^{-2} K^{-1}$]
k	conductivity [$W m^{-1} K^{-1}$]
L	length of tubes (heat transfer surface) [m]
M	number of experimental points
m_2	constant
N	number of tube-side passes
NTU	number of transfer units, $U A/\dot{W}$
n	number of tubes
P	dimensionless temperature change
Pe	Péclet number
R_1	ratio of thermal flow rate, $\dot{W}_1/\dot{W}_2$
Re_1	shell-side Reynolds number, based on ref. [14]
Re_1^*	shell-side Reynolds number, based on d_a and maximum fluid velocity
S	distance between baffles [m]
s	tube wall thickness [m]
T	dimensionless shell-side fluid temperature, $(\vartheta_1-\vartheta_2')/(\vartheta_1'-\vartheta_2')$
t_j	dimensionless tube-side fluid temperature, $(\vartheta_{2,j}-\vartheta_2')/(\vartheta_1'-\vartheta_2')$
U	overall heat transfer coefficient [$W m^{-2} K^{-1}$]
U^*	apparent overall heat transfer coefficient [$W m^{-2} K^{-1}$]
$\dot{V}$	volumetric flow rate [$m^3 s^{-1}$]
$\dot{W}$	thermal flow rate [$W K^{-1}$]
X	axial coordinate [m]
x	dimensionless axial coordinate, X/L
y	dummy variable
Z	pitch ratio.

Greek symbols

δ	clearance between baffles and shell [m]
ε_j	ratio of $(NTU_2)_j$ in tube pass j to the total NTU_2 of the exchanger
μ	fluid viscosity [$kg m^{-1} s^{-1}$]
ν	fluid kinematic viscosity [$m^2 s^{-1}$]
ρ	fluid density [$kg m^{-3}$]
ϑ	fluid temperature [K]
$\Delta\vartheta_{a,b}$	fluid temperature difference at the ends of the exchanger [K]
$\Delta\vartheta_{mlog}$	log-mean temperature difference (LMTD) [K].

Subscripts

m	mean value
w	wall
1	shell-side
2	tube-side.

Superscripts

$'$	inlet
$''$	outlet.

according to need. In front of the test heat exchanger, the water is completely mixed in a buffer reservoir (B2). The water in the cold cycle is transported by the greater centrifugal pump (P1). The heated water from the test heat exchanger is cooled down by the plate heat exchanger (W2), which receives the low temperature cooling water from the ground with an adjustable valve. The cooled water is completely mixed in another buffer reservoir (B1) before entering the test heat exchanger. To avoid overpressure in both cycles, each cycle is connected independently to its own overhead reservoir (B), which is open to the atmosphere.

Test heat exchanger

For the variation of distance between baffles and clearance between baffles and shell, a test shell-and-tube heat exchanger with exchangeable baffles is designed and constructed. The inside shell diameter is 210 mm with an effective heat exchange length of 1650 mm. The tubes and the shell are made of stainless material. The tubes have an inside diameter of 10 mm and outside diameter of 12 mm. Figure 2 shows the schematic of the tube bundle containing 92 tubes with pitch ratio of 1.5. Baffles with various diameters but with a constant thickness of 2 mm and cutoff of 50 mm were constructed to adjust the clearance between baffles and shell. The distance between baffles is varied through different length screws fixed between baffles.

Data acquisition and control

The inlet temperatures of the test heat exchanger, as well as the temperature changes between inlets and outlets are measured with NiCr–Ni thermocouples. The pressure drop and volumetric flow rate on both shell and tube sides are measured with pressure difference transformers and turbine flow meters, respectively. All the measurements are controlled and acquired with a data acquisition/control unit (HP 3852A) and a universal counter (HP 5334A) interfaced via IEC-bus to a personal computer (Compaq). Thermal performance with four different clearances between shell and baffles, i.e. 0.2, 1.0, 2.0 and 3.0 mm, and two different distances between baffles, i.e. 81 and 219 mm, were investigated. Under each clearance and distance, experiments with cocurrent flow as well as

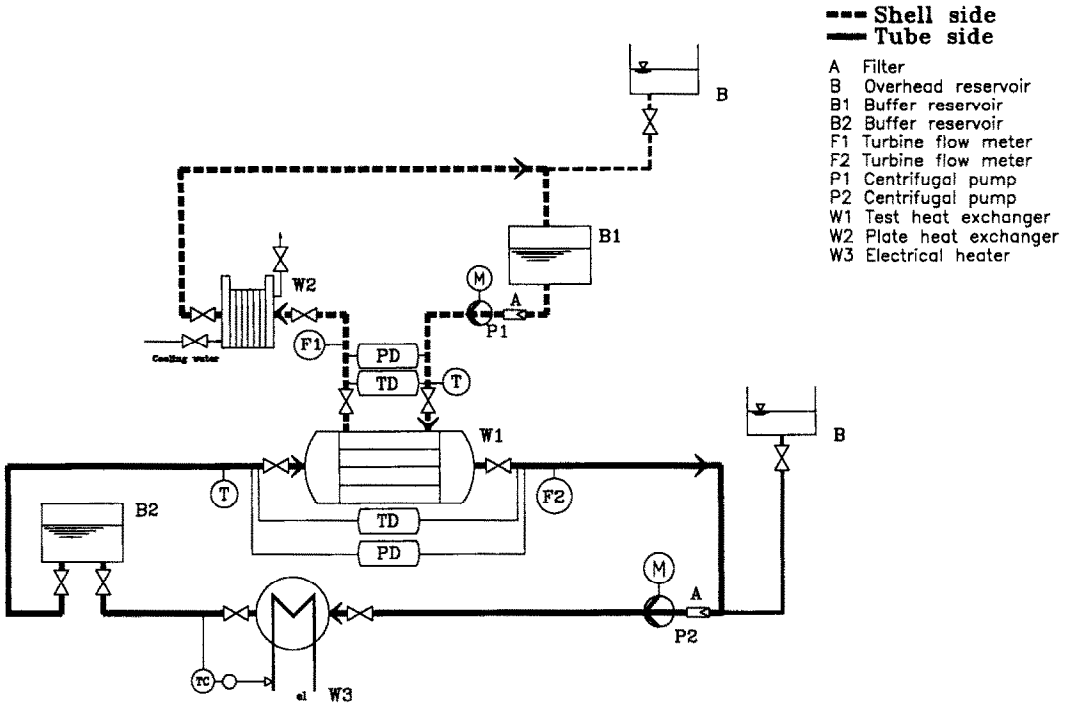

FIG. 1. Overall experimental setup.

countercurrent flow at 28 different operating points, with the volumetric flow rate on the shell-side from 0.5 to 2.0 l s^{-1}, and tube side from 2.0 to 3.5 l s^{-1} were measured. The arithmetic mean temperature on the shell-side was adjusted at 30°C and on the tube-side at 40°C for all experiments. Because of shortage of time, the experiments with a shell–baffle clearance of 1.0 mm and a distance between baffles of 219 mm were skipped.

Data reduction

From the measured data, the dimensionless temperature change on the shell-side (P_1) and the appar-

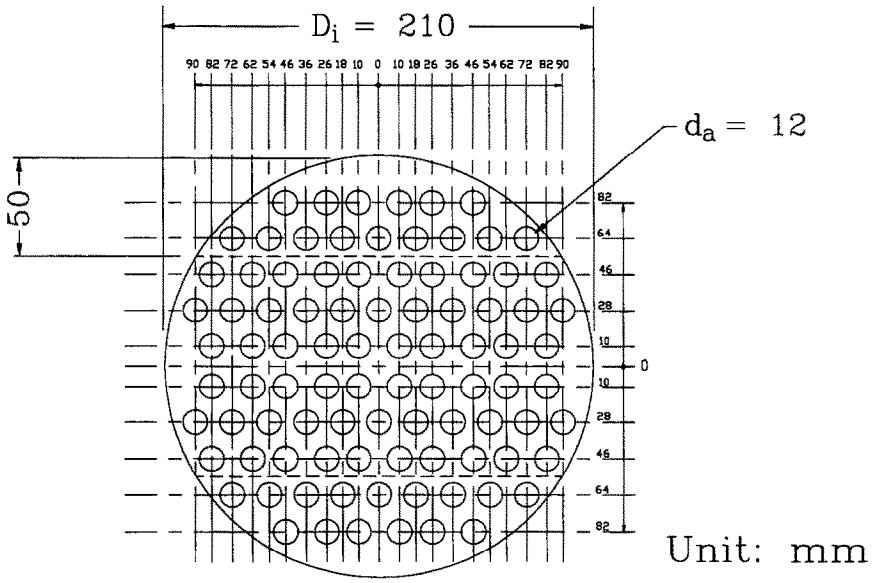

FIG. 2. Schematic of tube bundle arrangement.

ent overall heat transfer coefficient (U^*) are calculated, which are defined as follows:

$$P_1 = \frac{\vartheta_1' - \vartheta_1''}{\vartheta_1' - \vartheta_2'} \tag{1}$$

$$U^* = \frac{\dot{W}_2(\vartheta_2' - \vartheta_2'')}{A\Delta\vartheta_{\text{mlog}}} \tag{2}$$

with the log-mean temperature difference (LMTD)

$$\Delta\vartheta_{\text{mlog}} = \frac{\Delta\vartheta_a - \Delta\vartheta_b}{\ln(\Delta\vartheta_a/\Delta\vartheta_b)} \tag{3}$$

where $\Delta\vartheta_a$ and $\Delta\vartheta_b$ are the fluid temperature differences at the ends of the exchanger. The Reynolds number on the shell side is calculated according to the definition from VDI-Wärmeatlas [14]

$$Re_1 = \frac{\pi d_a \rho_{1m} \dot{V}_1}{2(1-\pi/4Z)D_i S \mu_{1m}} \tag{4}$$

with the properties ρ_{1m} and μ_{1m} at the arithmetic mean temperature $\vartheta_{1m} = (\vartheta_1' + \vartheta_1'')/2$. The tube-side Reynolds number is calculated as usual

$$Re_2 = \frac{\dot{V}_2 d_i}{\pi n (d_i/2)^2 \nu_{2m}} \tag{5}$$

with the volumetric flow rate and the kinematic viscosity ν_{2m} at the arithmetic mean temperature $\vartheta_{2m} = (\vartheta_2' + \vartheta_2'')/2$.

Uncertainty analysis

In each experimental point, the uncertainty was calculated and analyzed extensively with square forward-difference method, recommended by Profos [15]. The maximum uncertainty of the apparent overall heat transfer coefficient U^*, which appears when the shell-side flow rate is small (i.e. the log-mean temperature is small), is $\pm 4\%$ with countercurrent flow and $\pm 6\%$ with cocurrent flow. The Reynolds numbers were determined with maximum uncertainties of ± 2.0 and $\pm 0.8\%$ on the shell-side and tube-side, respectively.

AXIAL DISPERSION MODEL

To consider the deviation from the ideal axial plug flow on the shell-side with completely transversely mixing in any cross-section, a model with axial dispersion is used. Numerous investigations about this model have been carried out for modeling chemical reactors [16], porous media [17], packed beds [18] and shell-and-tube heat exchangers [9–13]. One extra parameter, the Péclet number Pe, is introduced in the dimensionless energy balance of the shell-side stream as an empirical parameter

$$Pe = \frac{\dot{W}_1 L}{E A^*} \tag{6}$$

where E is the dispersive axial thermal conductivity. Two different arrangements are possible in the multipass shell-and-tube heat exchanger. The arrangement I has the first tube-side pass in countercurrent flow to the shell-side stream and the arrangement II has conversely the first tube-side pass in cocurrent flow. Under the assumptions of uniform overall heat transfer coefficients within each tube pass, the NTU ratio ε_j, which is defined as the ratio of the number of transfer units from pass j to that of the whole exchanger, is introduced in the energy balance differential equations [19].

Introducing the axial dispersion on the shell-side and with the assumptions of constant fluid properties, steady state condition and neglecting heat losses to the surroundings, the differential energy balance equations can be expressed as

$$\frac{1}{Pe}\frac{d^2T}{dx^2} - \frac{dT}{dx} = \pm\frac{1}{R_1}\sum_{j=1}^{N}(-1)^j \cdot \frac{dt_j}{dx} \tag{7}$$

and

$$\varepsilon_j NTU_2 (T - t_j) = \pm(-1)^j \cdot \frac{dt_j}{dx}; \quad j = 1, \ldots, N \tag{8}$$

where the positive sign(+) of sign ($\pm$) is for arrangement I and the negative (−) for arrangement II. The corresponding boundary conditions are

Arrangement I:

$$x = 1, \quad t_1 = 0 \tag{9}$$

$$x = 0, \quad t_j = t_{j-1} \tag{10}$$

$$x = 1, \quad t_{j+1} = t_j \tag{11}$$

$$j = 2, 4, 6, \ldots$$

Arrangement II:

$$x = 0, \quad t_1 = 0 \tag{12}$$

$$x = 0, \quad t_{j+1} = t_j \tag{13}$$

$$x = 1, \quad t_j = t_{j-1} \tag{14}$$

$$j = 2, 4, 6, \ldots$$

For both arrangements, the boundary conditions of Danckwerts [20] fulfil the overall energy balance

$$\left.\frac{1}{Pe}\frac{dT}{dx}\right|_{x=0^+} = T|_{x=0^+} - 1 \tag{15}$$

$$\left.\frac{1}{Pe}\frac{dT}{dx}\right|_{x=1} = 0. \tag{16}$$

The general solutions of this system are shown in ref. [21]. In this paper, the experimental investigation will concentrate on single-pass cocurrent and countercurrent flow with different clearances between baffles and shell, as well as with different distances between baffles. For cocurrent flow ($N = 1$, arrangement II), the shell-side dimensionless temperature change P_1 is [21]

$$P_1 = \frac{NTU_1[Pe\,y_2(1-e^{y_1})-y_1y_2-y_1(Pe\,(1-e^{y_2})-y_2)\,e^{(y_1-y_2)}]}{y_1y_2[(y_1-NTU_1-Pe)-(y_2-NTU_1-Pe)\,e^{(y_1-y_2)}]} \tag{17}$$

with

$$y_{1,2} = 0.5(Pe+R_1NTU_1 \pm\sqrt{[(Pe-R_1NTU_1)^2+4Pe\,NTU_1(1+R_1)]})$$

where the positive sign (+) of sign (±) refers to y_1 and the negative one to y_2.

For countercurrent flow ($N = 1$, arrangement I)

For $R_1 \neq 1$

$$\frac{1}{P_1} = 1+\frac{y_1y_2(y_1-y_2)\,e^{y_1}}{NTU_1[y_2Pe-y_1y_2+Pe\,(y_1-y_2)\,e^{y_1}+y_1(y_2-Pe)\,e^{(y_1-y_2)}]} \tag{18}$$

with

$$y_{1,2} = 0.5(Pe+R_1NTU_1 \pm\sqrt{[(Pe+R_1NTU_1)^2-4Pe\,NTU_1(R_1-1)]})$$

and sign (±) as defined above.

For $R_1 = 1$

$$\frac{1}{P_1} = 1+\frac{(Pe+NTU_1)^2}{NTU_1[Pe^2+NTU_1(1+Pe-e^{-(Pe+NTU_1)})]}. \tag{19}$$

Based on the heat transfer surface area A_1, the overall heat transfer coefficient in the shell-and-tube heat exchanger

$$U = \frac{1}{(1/h_1)+(s/k_w)(A_1/A_m)+(1/h_2)(A_1/A_2)} \tag{20}$$

where $A_1 = n\pi d_a$, $A_2 = n\pi d_i$ and $A_m = (A_1-A_2)/\ln(A_1/A_2)$. The heat transfer coefficient on the shell- and tube-sides are calculated using the following formulas [22, 10]:

$$h_1 = C_1\,Re_1^{0.6}\,Pr_1^{0.36}\frac{k_1}{(\pi d_a/2)} \tag{21}$$

$$h_2 = C_2\,Re_2^{m_2}\,Pr_2^{1/3}\frac{k_2}{d_i}. \tag{22}$$

Table 1. Result of minimization

Distance between baffles	81 mm	219 mm
C_1	0.556516	0.562061
C_2	0.021962	0.022165
m_2	0.796283	0.801559
Pe for δ = 0.2 (mm)	30.58	38.00
δ = 1.0	25.34	—
δ = 2.0	21.35	35.81
δ = 3.0	10.94	11.27

Using experimental data in an objective function, defined as follows, the constants C_1, C_2 and m_2 can be determined together with the unknown dimensionless dispersion coefficient, the Péclet number Pe, through a minimization process from Gill *et al.* [23].

$$\sum_{i=1}^{M}(P_{1,calc}-P_{1,exp})_i^2 \to \min$$

where the $P_{1,calc}$ is calculated from equations (17)–(19) with the boundary conditions from ref. [20]. For each minimization, all the experimental data with same distance between baffles, with different clearances between baffles and shell, and with different stream flow directions have been taken into consideration. Through minimization, the unknown constants C_1, C_2, m_2 and corresponding Péclet numbers can be determined. The results are shown in Table 1.

RESULTS AND DISCUSSION

Figures 3 and 4 show the experimental values of U^* for countercurrent flow under different distances between baffles and different tube-side Reynolds numbers. For different distances, the U^* curves connect smoothly when the clearance between baffles and shell is small (δ = 0.2 mm). However, when the clearance increases, the U^* curves do not connect smoothly for different distances, as shown in Fig. 4 (δ = 3.0 mm). This shows that the apparent overall heat transfer coefficient is strongly influenced by the leakage between baffles and shell.

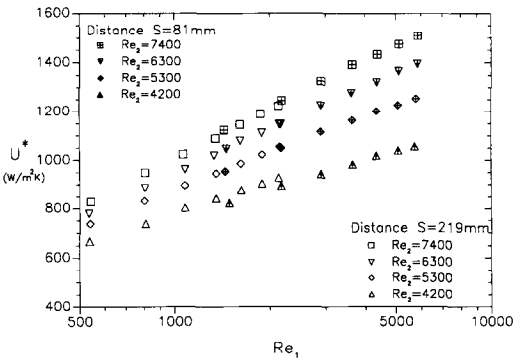

FIG. 3. U^* for different distances between baffles, with δ = 0.2 mm, countercurrent flow.

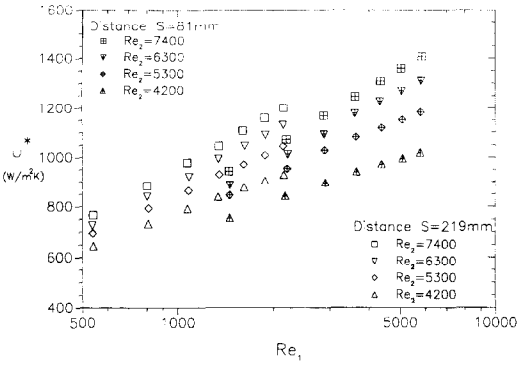

FIG. 4. U^* for different distances between baffles, with $\delta = 3.0$ mm, countercurrent flow.

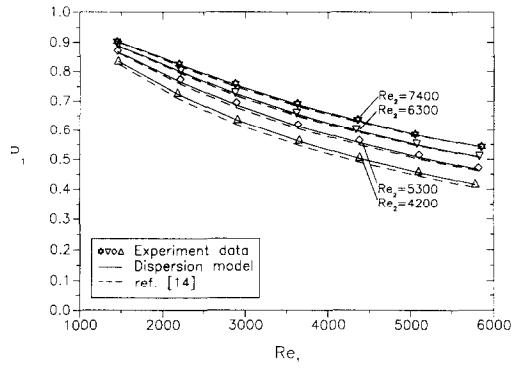

FIG. 5. Comparison of dimensionless temperature change P_1 for $S = 81$ mm, $\delta = 3.0$ mm, countercurrent flow.

In Figs. 5 and 6, the calculated and measured dimensionless temperature changes P_1 are presented as a function of both Reynolds numbers. The solid lines are calculated according to the dispersion model using equations (17)–(22) together with the data of Table 1. Nearly the same curves are obtained if the mean values $C_1 = 0.56$, $C_2 = 0.022$ and $m_2 = 0.8$ are used for both distances between baffles. The dashed lines are calculated with the method recommended in the VDI-Wärmeatlas [14]. The symbols represent the experimental values of P_1 for the four different tube-side Reynolds numbers. The wall viscosity correction was included in the calculation of the heat transfer

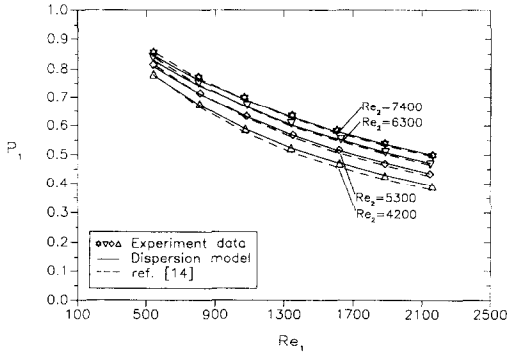

FIG. 6. Comparison of dimensionless temperature change P_1, for $S = 219$ mm, $\delta = 3.0$ mm, countercurrent flow.

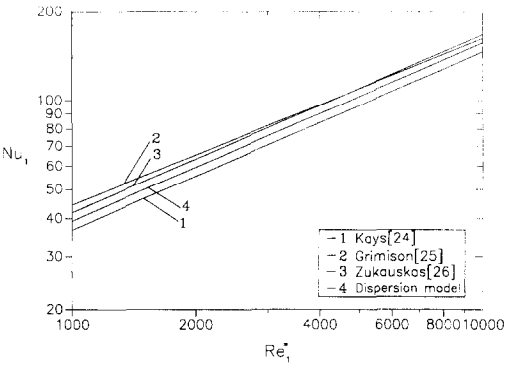

FIG. 7. Comparison of calculation of Nu from dispersion model and refs. [24–26].

coefficients. Figures 5 and 6 show that the dispersion model can very accurately predict the experimental data with the unique set of heat transfer correlations. Also the method of the VDI-Wärmeatlas yields good results.

The constant C_1, which depends on the tube bundle geometry, assumes a value of 0.56. This value is valid for different shell–baffle clearances and different distances between baffles. The divergent thermal performance caused by leakage or bypass effects is taken into account by the Péclet number. The common constant C_1 obtained from the minimization process clearly indicates that the distance between baffles has no influence on C_1. Compared to other results [24–26], the calculated shell-side mean Nusselt numbers, shown in Fig. 7, compare well with other equations within a range of ± 5–7%.

In the range of experimental tube-side Reynolds numbers from 4200 to 7400, the constants in the heat transfer equation (equation (22)), C_2 and m_2 have a value of 0.022 and 0.80, respectively, which are similar to numerous investigations [27–29].

The Péclet number Pe, which contains an apparent dispersive thermal conductivity E in axial flow direction, is a function only of distance between baffles and of the clearance between baffles and shell. It does not depend on the Reynolds number, as also can be concluded from the results of Xuan and Roetzel [10–12]. The calculated Péclet numbers from Table 1

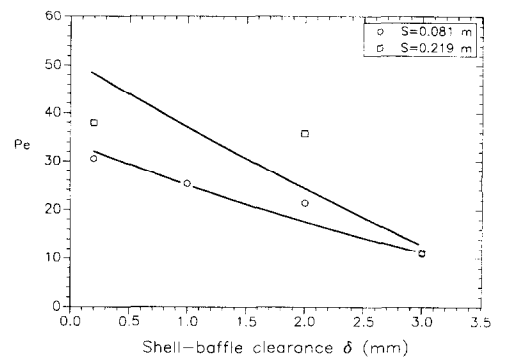

FIG. 8. Calculated Péclet number Pe from Table 1.

are displayed as symbols in Fig. 8, while the solid lines represent possible functions between Péclet number and shell–baffle clearance. When the clearance between baffles and shell increases, which indicates the increase of the axial dispersion effect caused by leakage and bypassing, the Péclet number Pe decreases. High values $Pe > 40$ have nearly the same effect as an infinite value $Pe = \infty$ and the ideal plug flow model applies. Thus, experimentally determined high Péclet numbers are inaccurate in the region $Pe > 40$. Further experiments will be needed to determine exactly the dependence of Péclet number on geometry.

CONCLUSIONS

(1) The shell–baffle leakage, i.e. flow through the clearance between shell and baffles has great influence on the apparent overall heat transfer coefficient U^*, which is based on the ideal plug flow model. The coefficient shows a reduction up to 7% at $Re_1 = 5800$ and 16% at $Re_1 = 1450$ between clearance 0.2 mm ($\delta/D_i = 0.000952$) and clearance 3.0 mm ($\delta/D_i = 0.0143$). This reduction will be even greater when the tube-side Reynolds number Re_2 increases.

(2) With the axial dispersion model, the dimensionless temperature change P_1 can be predicted in a simpler way than with other methods. For different clearances between baffles and shell as well as different distances between baffles, one unique set of heat transfer correlations can describe all experimental results, when the Péclet number is introduced to account for the effect of shell-side maldistribution. The Péclet number depends only on the geometry and not on the Reynolds number. However, this must be verified by further experiments.

Acknowledgements—The authors would like to express their thanks to the Deutsche Forschungsgemeinschaft for the financial support of this research work.

REFERENCES

1. K. Gardner and J. Taborek, Mean temperature difference: a reappraisal, *A.I.Ch.E. Jl* **23,** 777–786 (1977).
2. T. Tinker, Shell side characteristics of shell and tube heat exchangers, parts I, II and III, *General Discussion on Heat Transfer*, IMechE, 89–116 (1951).
3. T. Tinker, Shell side characteristics of shell and tube heat exchangers—a simplified rating system for commercial heat exchangers, *Trans. ASME* **80,** 36–52 (1958).
4. J. W. Palen and J. Taborek, Solution of shell side flow pressure drop and heat transfer by stream analysis method, *Chem. Engng Prog. Symp. Ser.* **65**(92), 53–63 (1969).
5. A. C. Mueller, Effects of some types of maldistribution on the performance of heat exchangers, *Heat Transfer Engng* **8**(2), 75–86 (1987).
6. E. S. Gaddis and E. U. Schlünder, Einfluß der Leckströmung auf Temperaturverlauf und übertragbare Wärmemenge in Röhrenkesselapparaten mit Umlenkblechen, *Verfahrenstechnik* **10**(4), 191–194 (1976).
7. M. Diaz and A. T. Aguayo, How flow dispersion affects exchanger performance, *Hydrocarbon Processing* **66**(4), 57–60 (1987).
8. W. Roetzel and B. Spang, *Analytisches Verfahren zur thermischen Berechnung mehrgängiger Rohrbündelwärmeübertrager*, Fortschr.-Ber. VDI, Reihe 19, Nr. 18. VDI, Düsseldorf (1987).
9. B. Spang and W. Roetzel, Axial dispersion model for segmentally baffled shell and tube heat exchangers, Eurotherm Seminar No. 9, Bochum, 10–11 July 1989, *Entropie*, 99–104 (1991).
10. Y. Xuan, *Thermische Modellierung mehrgängiger Rohrbündelwärmeübertrager mit Umlenkblechen und geteiltem Mantelstrom*, Fortschr.-Ber. VDI, Reihe 19, Nr. 52. VDI, Düsseldorf (1991).
11. W. Roetzel and Y. Xuan, Dispersion model for split-flow heat exchangers. In *Recent Advances in Heat Transfer*, Proceedings of the First Baltic Heat Transfer Conference, Göteborg, Sweden, 26–28 August 1991 (Edited by B. Sundén and A. Zukauskas), pp. 561–575. Elsevier, Amsterdam (1992).
12. W. Roetzel and Y. Xuan, Dispersion model for divided-flow heat exchanger. In *Design and Operation of Heat Exchangers*, pp. 98–110. Springer, Berlin Heidelberg (1992).
13. W. Roetzel and Y. Xuan, Analysis of transient behaviour of multipass shell and tube heat exchangers with the dispersion model, *Int. J. Heat Mass Transfer* **35,** 2953–2963 (1992).
14. E. S. Gaddis and V. Gnielinski, Wärmeübertragung im Außenraum von Rohrbündelwärmeübertragern mit Umlenkblechen, *VDI-Wärmeatlas*, Abschnitt Gg, 6. Aufl. VDI, Düsselorf (1991).
15. P. Profos, *Meßfehler*, p. 101. Teubner, Stuttgart (1984).
16. C. Y. Wen and L. T. Fan, *Models for Flow Systems and Chemical Reactors*, Marcel Dekker, Inc., New York (1975).
17. J. Baer, Hydrodynamic dispersion in flow through porous media. In *Flow through Porous Media*, p. 109. Academic Press, R. J. M. De Wiest, New York (1969).
18. D. Vortmeyer, Packed bed thermal dispersion models and consistent sets of coefficients, *Chem. Engng Process* **26,** 263–268 (1989).
19. W. Roetzel and B. Spang, Thermal calculation of multipass shell and tube heat exchangers, *Chem. Engng Res. Des.* **67,** 115–120 (1989).
20. P. V. Danckwerts, Continuous flow systems, *Chem. Engng Sci.* **2,** 1–13 (1953).
21. B. Spang, *Über das thermische Verhalten von Rohrbündelwärmeübertragern mit Segmentumlenkblechen*, Fortschr.-Ber. VDI, Reihe 19, Nr. 48. VDI, Düsseldorf (1991).
22. A. Zukauskas and R. Ulinskas, *Heat Transfer in Tube Banks in Crossflow*, p. 93. Springer, Berlin (1988).
23. P. E. Gill, W. Murray and M. Wright, *Practical Optimization*, p. 94. Academic Press, New York (1982).
24. W. M. Kays and A. L. London, *Compact Heat Exchangers*, 3rd Edn, p. 146. McGraw-Hill, New York (1984).
25. E. D. Grimison, Correlation and utilization of new data on flow resistance and heat transfer for crossflow of gases over tube banks, *Trans. ASME* **59**(7), 583–594 (1937).
26. A. Zukauskas, Heat transfer from tubes in crossflow. In *Advances in Heat Transfer* (Edited by J. P. Hartnett and T. F. Irvine, Jr.), Vol. 8, pp. 93–160. Academic Press, New York (1972).
27. F. W. Dittus and L. M. K. Boelter, Heat transfer in automobile radiators of the tubular type, *Univ. Calif. Berkeley Publ. Engng* **2,** 443–461 (1930).
28. A. P. Colburn, A method of correlating forced convection heat transfer data and a comparison with fluid friction, *Trans. A.I.Ch.E.* **29,** 174–210 (1933).
29. E. N. Sieder and G. E. Tate, Heat transfer and pressure drop of liquids in tubes, *Ind. Engng Chem.* **28,** 1429–1435 (1936).